Stellar Distributions in Dark Matter Halos: Looking Over the Edge

Principal Investigator: Liese van Zee
Institution: Indiana University
Electronic mail: vanzee@astro.indiana.edu
Technical Contact: Daniel A Dale, University of Wyoming
Co−Investigators: Daniel A. Dale, University of Wyoming
Kate L. Barnes, Indiana University
Shawn Staudaher, University of Wyoming
Daniela Calzetti, University of Massachusetts
Julianne J. Dalcanton, University of Washington
James S. Bullock, University of California, Irvine
Rupali Chandar, University of Toledo
Science Category: Extragalactic: nearby galaxies (z<0.05, v_sys<15,000 km/s)
Observing Modes: IRAC Post−Cryo Mapping
Hours Requested: 1,005.3
Proprietary Period(days): 0

Abstract:
We propose to obtain deep observations with IRAC bands 1 and 2 to trace the faint extended stellar component of nearby galaxies. Little is known about the full extent of the stellar distribution in normal galaxies; deep IR observations of the area around galaxies will allow us to trace the stellar distribution to unprecedented levels. Our sample will include galaxies with a range of morphology, inclination angle, luminosity, and environment in order to explore fully the diverse range of galaxy properties and to enhance the legacy value of this data set. These observations will enable a wide variety of projects, including investigation of thick disks and halo formation, identification of old and young star clusters, and identification of stars well beyond the bright stellar disk. The proposed observations will provide not only a census, but also the first quantitative measurements of the physical properties of low surface brightness features identified around nearby galaxies (e.g., stellar mass surface density, distribution, and fraction of total stellar mass). With sensitivity to substructures featuring stellar mass surface densities of only a few x 0.01 M_sun/pc^2, this project will provide the first look at the stellar edge for a large sample of galaxies and will be instrumental in providing observational constraints for galaxy formation models.

1 Science Plan

1.1 Scientific Justification

1.1.1 Introduction

Deep imaging provides a unique opportunity to trace the baryonic content of the universe to low surface density in the outer regions of galaxies. Recently, Thilker et al. (2005) presented spectacular UV images which show evidence of star formation activity at radii 4 times the optical radius in M83 (Figure 1). Similarly, Ferguson et al. (1998) found star formation activity extending to at least twice the optical radius in NGC 628, NGC 1058, and NGC 6946. Recent deep imaging observations have also revealed faint stellar distributions that extend factors of 2-3 beyond the bright optical component in nearby galaxies (e.g., M31, Ibata et al. 2007; NGC 300, Bland-Hawthorn et al. 2005; NGC 5907, Martínez-Delgado et al. 2008). Indeed, based on the frequency of extended UV disks found around star–forming galaxies (∼25%), Zaritsky & Christlein (2007) infer that large diffuse stellar disks are a common feature in the local Universe.

The existence of extended, low-surface brightness components around bright galaxies provides an important opportunity for constraining modern structure formation models. Perhaps the most robust prediction of ΛCDM-based galaxy formation is that bright galaxies should undergo frequent (statistically quantifiable) minor mergers with objects that are much less luminous than the primary system (e.g., Stewart et al. 2008, and references therein; Peñarrubia et al. 2006). Though the morphological signatures of these small ($m/M \sim 1/20$) mergers are necessarily less dramatic than those of major mergers, they are expected to be much more common. The numbers of tidal streams from accreted stars provide direct constraints on the rate of these low-mass accretion events (Johnston et al. 2001). Moreover, interactions with low-luminosity (dark) substructures can induce a number of observable low-surface brightness features including flares, rings, thickened disk components, and anti-truncations (Abadi et al. 2006; Kazantzidis et al. 2008; Younger et al. 2007).

The results of observations and simulations therefore suggest that galaxies are much larger entities than one might expect based on their high surface brightness components alone. Indeed, these recent discoveries motivate an increased need to understand galaxy formation and the growth of galaxy disks in the context of the wide range of galaxy properties observed today. We propose deep wide-field infrared observations of a large statistical sample of galaxies to trace the full extent of the stellar component in normal galaxies in order to understand the distribution of baryons in nearby systems.

1.1.2 Science Goals

The deep infrared observations required for studies of the extended stellar distribution in nearby galaxies will permit a multitude of studies. We highlight a few of our primary science goals below, with an emphasis on the projects to be addressed by our team.

•Extended Stellar Distributions Around Normal Galaxies

Understanding the nature and extent of stellar populations around nearby galaxies is the primary science driver for the proposed observations. While the inner parts of galaxies are characterized by rapid mixing and orbital migration (e.g., Roškar et al. 2008), the outer regions of galaxies are characterized by long dynamical times. Structure can therefore persist for many Gigayears at large radii, leaving a long-lived fingerprint of the past stellar accretion

and structural evolution of a galaxy. These structures can be readily seen in ΛCDM simulations of hierarchical galaxy formation (e.g., Johnston et al. 2001; Bullock & Johnston 2005), and their number and amplitude can potentially provide strong constraints on the epoch of reionization (e.g., Bekki & Chiba 2005). Unfortunately, these structures are difficult to observe directly, due to their low characteristic surface brightnesses.

In spite of the difficulty in detection, we do know that complicated outer structures exist in some galaxies. A rich degree of substructure has been revealed in the Milky Way and M31 in maps of the density of resolved stars (e.g., Ivezić et al. 2008; Ibata et al. 2007), as well as in nearby spiral galaxies from deep optical surface photometry (Martínez-Delgado et al. 2008, 2010; Zheng et al. 1999). These structures, such as those found wrapping around NGC 5907 (Figure 1) or M31, can be modelled as debris from low-mass satellite accretion during growth of the galaxy's disk (Martínez-Delgado et al. 2008). The stars in the outer galaxy therefore are encoding remnants of the hierarchical merging characteristic of ΛCDM. Unfortunately, mapping extended halos and substructure with individual stars is limited to the nearest systems, and the ultra-wide photometry used for nearby galaxies such as NGC 5907 gives no constraints on the actual masses involved in the observed streams. **With our proposed observations, we can systematically constrain the prevalence of substructure as a function of *stellar mass* to surface mass density levels of a few $\times$ 0.01 $M_\odot$ pc^{-2}.**

While it is quite evident that mergers and accretion can yield faint extended stellar distributions, not all faint emission around galaxies is necessarily the result of tidal stirring or accretion. Indeed, several galaxies have been identified recently with well-ordered extended HI disks – factors of 2-10 times the optical size – and evidence of star formation at large radii (e.g., NGC 628, Ferguson et al. 1998; UGC 5288, Figure 2). For example, the extended UV disk around M83 shows hot spots of recent star formation (e.g., Thilker et al. 2005) that are accompanied by dust emission visible in deep IR observations (Dong et al. 2008). These recent observational results highlight our need to explain how extended star-forming gas disks survive to the present epoch – are they replenished by additional gas-rich accretion events? has previous star formation been suppressed due to star formation threshold effects in high angular momentum disks? are the extended disks induced by tidal interactions? Observations of the frequency, extent, and distribution of the faint stellar populations around nearby galaxies are crucial for characterizing the growth of galaxy disks, both by accretion of satellites and by *in situ* star formation activity.

Interestingly, these two disk growth mechanisms have distinctly different predictions for the age of the associated extended stellar population. For accretion scenarios, the diffuse stellar distribution is largely composed of the remnants of previously accreted satellites, and thus is dominated by an old stellar population (e.g., Abadi et al. 2006). Conversely, inside-out galaxy formation models predict that the outer disk should be dominated by young stellar populations as the diffuse outer gas disk is slowly converted into stars (e.g., Roškar et al. 2008). Optical/UV detection of these extended optical disks is biased towards the younger, star forming disks, as those dominated by older stellar populations will be more difficult to detect at a fixed stellar surface density. **Our proposed *Spitzer* observations will be sensitive to faint stellar populations regardless of the galaxy's star formation history.**

In particular, the proposed deep *Spitzer* observations will be *an order of magnitude* more sensitive than typical surveys of nearby galaxies (i.e., LVL, SINGS, and S^{4}G, Dale et al. 2009; Kennicutt et al. 2003; Sheth et al. 2010), which already reach depths where the stellar disk can be traced to 2-3R_{25} (e.g., Regan et al. 2006). As illustrated in Figures 2 and 3, the

expected surface brightness limit of the proposed *Spitzer* observations is comparable to an optical (B-band) surface brightness limit of ∼30 mag arcsec^{-2} for an old stellar population. While such depths are possible in the optical theoretically, in practice the systematic uncertainties in flat-fielding, sky subtraction, and scattered light make this project impossible at optical wavelengths even with 10s of hours of observing time per field. **In other words, the proposed *Spitzer* 3.6μm imaging will provide the first comprehensive census of the extent, distribution, and nature of extended stellar distributions around normal nearby galaxies, to stellar surface density limits that are unreachable from the ground.**

Our observations will permit the first detailed analysis of the structure and morphology of the stellar distribution to very large radii, and thus provide stringent tests for ΛCDM models of disk growth and galaxy evolution. For example: is there evidence of stellar streams in the low surface brightness disk (accretion)? is the distribution indicative of axisymmetric *in situ* growth? is the radial extent correlated with disk angular momentum or dark matter fraction (*in situ* growth)? is the radial extent correlated with bulge-to-disk ratio (accretion)? Once outer structures are identified, follow-up targeted observations with GALEX or HST can further constrain the colors and mean stellar ages of higher surface brightness structures in the outer disk, and therefore provide additional constraints on galaxy formation and disk growth.

Given how little is known about stellar structure at these surface density limits, we are specifically targeting galaxies with a wide range of morphology and luminosity (Figure 4). The sample will therefore allow us to probe our expectation that the extent and type of faint stellar population should be related to both the depth of the dark matter potential well and to global galaxy properties such as bulge-to-disk ratio. The existing data already suggest that the properties of outer disks may vary substantially within the galaxy population, even at the higher surface brightnesses reachable with current ground-based observations. Color gradients in the outer disk range from the typical blue color gradients found in spiral galaxies (e.g., Markarian et al. 1965), to red gradients in gas-rich dwarf irregular galaxies (e.g., Dohm Palmer et al. 1998). These differences may be associated with observed variation in the properties of extended gaseous disks, which are more commonly associated with late-type galaxies (e.g., DDO 154, Carignan & Purton 1998; UGC 5288, Figure 2). These variations may be due to differences in merger history among high and low mass galaxies (e.g., Bekki 2008), or these trends may be indicative of a transition in galaxy disk growth from high mass to low mass systems, just as there is an apparent transition between star formation modes/efficiency in the inner disk of low and high mass spirals (e.g., van Zee et al. 1997). Regardless of the origin of these differences, **the size and breadth of our proposed sample will allow us to take the first steps in quantifying the differences among low and high mass spirals, and early– and late–type galaxies, thus providing an important foundation for understanding the extended stellar halos of galaxies.**

•The Origins of Disk Truncations

Surface brightness profile fitting of edge-on galaxies routinely shows a diversity of outer profile shapes, including truncations, smooth exponentials, or even "anti-truncations" (e.g., Kregel & van der Kruit 2004; Pohlen & Trujillo 2006). However, it is unclear whether these changes in the surface brightness profile reflect true changes in the underlying stellar mass distribution. Studies of individual resolved stars in NGC 4244 (de Jong et al. 2007) suggest that disk truncations are experienced by both old and young stellar populations in this

particular system, but there are less than a handful of other galaxies in which similar studies can be done. Moreover, studies of disk truncation and anti-truncation have been limited to edge-on systems, making it nearly impossible to correlate the slope changes with other structural features like spiral arms; such a connection would suggest a dynamical origin for the truncation (as in Roškar et al. 2008) rather than a star formation threshold (e.g., van den Bosch 2001). Only with deep NIR maps at low surface brightness can we expect to find evidence for disk truncations in the stellar masses of *face-on* systems.

The exploration of outer disk profile behavior in both face-on and edge-on systems will provide an important avenue for testing competing scenarios. Kazantzidis et al. (2008) have used N-body simulations to show that cosmologically-predicted satellite interactions tend to excite outer disk stars preferentially away from the disk plane, creating symmetric flares and generating apparent truncations when disks are viewed edge on (but not when viewed face-on; Kazantzidis et al. 2008). Younger et al. (2007) have argued that merger-driven gas inflow can produce anti-truncated disks when viewed face-on. Alternatively, if disk truncations are a consequence of the fall-off in gas surface density and the redistribution of stellar mass by secular processes (Roškar et al. 2008), then there should be no viewing angle dependence. Exploring the radial profiles of old stars in particular, will test the hypothesis that observed breaks are due to a radial change in stellar populations rather than a physical break in the distribution of mass (Bakos et al. 2008).

•Disk Scale Heights

Among the most troubling concerns with ΛCDM is that the predicted mergers will thicken disks to a degree that surpasses what we see directly in the Milky Way (Toth & Ostriker 1992; Navarro & Steinmetz 1997; Governato et al. 2007; Kazantzidis et al. 2008). A quantification of old disk scale heights in a large sample of galaxies will provide an important constraint on frequency and nature of ancient accretion events. While some progress on this issue has been made from the ground (e.g., Kregel et al. 2002, 2005; Yoachim & Dalcanton 2006) firm conclusions have been stymied by the presence of dust lanes, which are visible even in K-band imaging. Because of our inability to probe to the midplane of the galaxy with existing imaging, we have substantial uncertainties about the total surface density profile, and scale height of galactic disks, as a function of radius. In contrast, the 3.6μm imaging we are proposing here should be a superb probe of the midplane stellar mass density, giving us an unbiased measure of the scale height in old stars in systems spanning the full range of disk morphology and mass.

•Structure of Normal Galaxies

Although our main scientific emphasis is on outer disks and regions of low stellar density, our proposed observations will also yield superb deep, uniform images of the stellar mass distribution and structure for a representative sample of nearby galaxies. The 3.6μm and 4.5μm images probe the low mass stellar populations, and thus will be directly proportional to the stellar mass in the galaxy, *irrespective of the star formation history.* With our stellar maps, we will measure non–axisymmetric structural parameters like the strength of the stellar bar or the spiral structure, which are probes of a galaxy's dynamical history (Buta et al. 2004). We will also measure more 'classical' axisymmetric parameters, such as the bulge–to–disk ratio, galactocentric light profiles, etc. These structural parameters play a pivotal role in informing our understanding of galaxy evolution and the formation of the Hubble sequence (Kormendy & Kennicutt 2004). More importantly, we will be able to search for correlations between the easily-measured high surface brightness features (bar strength, contrast of spiral

arms, etc) and the faint structures seen in the outskirts. This comparison may allow us to link the dynamical evolution of the inner and outer regions. **With their sensitivity to old stars and their insensitivity to dust, the proposed IRAC observations will offer a view of the underlying stellar mass distribution that is unbiased by extinction or star formation history.**

•Stellar Cluster Populations in the Outskirts of Normal Galaxies

In addition to extended stellar disks, we will detect both young and old star clusters associated with the host galaxies. Indeed, we expect to find a large distribution of globular clusters around most galaxies, with particularly extended distributions in fields containing early-type galaxies. We also expect to identify young ($\tau \leq 1$ Gyr) star clusters; since many stars form in clusters (e.g., Carpenter 2000; Lada & Lada 2003), these star clusters will trace *in situ* star formation activity throughout the disk. We will use multi-wavelength spectral energy distribution (SED) fitting both to separate star clusters from contaminants, such as foreground stars and background galaxies, and to estimate cluster properties such as age, mass, and extinction (e.g., Dong et al. 2008; Alberts et al. 2011). Specifically, we will extract a point source catalog for every field to be combined with available multi-wavelength data (from UV to the optical). The near-IR fluxes from *Spitzer* 3.6μm and 4.5μm imaging observations are crucial to our efforts to disentangle age-metallicity-extinction degeneracies for each candidate star cluster. The proposed wide-field ($5 \times R_{25}$) observations will thus allow us to determine, for the first time, the shape of the cluster mass function in these extremely low surface density regions, which can then be compared with the typical power–law mass function ($\psi(M) \propto M^{\beta}$, with $\beta \sim -2$) observed for clusters formed within the optically luminous portions of star-forming galaxies (e.g., Fall et al. 2009; Chandar et al. 2010a,b). The masses and ages of the clusters will also allow us to assess the ability of star clusters to remain gravitationally bound in the outskirts of galaxies. These results will be compared with those found in the main body of galaxies (e.g., Fall, Chandar, & Whitmore 2005) to determine whether similar physical processes dominate in different galaxy environments.

1.1.3 Why *Spitzer*?

Observations of the faint outer disk are technically challenging at any wavelength (see, e.g., de Jong 2008). However, deep wide-field infrared imaging observations with *Spitzer* will provide a unique opportunity *to identify and measure quantitatively* the extent and physical parameters of the stellar mass distribution associated with normal galaxies. Similar near-IR observations are impossible to attempt from ground–based observatories due to the systematic and technical difficulties produced by varying sky levels and instruments with small areal coverage. Further, comparable ground–based optical imaging is biased toward younger, star forming disks and thus requires significantly longer integration times to achieve similar sensitivity to stellar mass; for instance, to image an old stellar population, R-band imaging on a 4-m class telescope will require ∼50 times the integration time to achieve similar depth as *Spitzer* 3.6μm imaging (Figure 2). Furthermore, even if the diffuse stellar populations can be detected in the optical, conversion from observed optical surface brightness to stellar mass density is highly dependent on the assumed stellar population age, initial mass function, and metallicity. Thus, observations with *Spitzer* are the only possible approach that will allow us to trace the stellar distribution in normal galaxies to unprecedented levels at wavelengths that are insensitive to both dust extinction and the galaxy's star formation history.

1.2 Technical Plan

1.2.1 Sample Definition

We have identified a large statistical sample of galaxies (92) for this project in order to explore the properties of the faint stellar distributions associated with galaxies with a wide range of physical properties and possible formation histories. Indeed, due to the exploratory nature of this project, it is necessary to include several galaxies of each morphological type, luminosity, and inclination angle in order to explore the relationships between the extended stellar distribution and global properties of the galaxies. The selected galaxies are drawn from a parent sample that includes all galaxies listed in NED with velocities less than 3000 km s^{-1} and $|b| > 20°$. Our primary selection criteria include both a minimum and maximum distance cut (2 Mpc < d < 15 Mpc), a minimum and maximum angular size cut ($2' < D_{25} < 13'$), an apparent magnitude limit ($m_B < 16.$), and a very strict galactic latitude constraint ($|b| > 60°$). The latter criterion has been imposed based on our experience with data from our pilot projects in Cycle 6, where we discovered that even moderate galactic latitude fields have significant contamination by foreground stars at the depths of these images. In addition, to minimize confusion with background structure, we exclude all potential targets within 20° of the center of the Virgo cluster. Note that the combination of our distance cut and apparent magnitude limit results in a nearly complete parent sample for galaxies brighter than M_B of −15; thus, in order to maintain a nearly complete parent sample while still including a representative sample of low mass galaxies, we further limit the sample to those galaxies brighter than M_B of −14. This final selection criterion ensures that the majority of galaxies in this sample are representative of systems that encompass the majority of baryonic mass in this volume element.

The volume element for this survey is selected to optimize our ability to identify and trace extended stellar components within the observational constraints of *Spitzer* and other telescopes. Specifically, we exclude galaxies within 2 Mpc of the Milky Way since both the primary target and any associated stellar streams will be too large to map efficiently with IRAC (expected angular sizes are several to tens of degrees). We also impose a maximum distance constraint (v < 1100 km s^{-1}, assuming H_0 of 72 km s^{-1} Mpc^{-1}) to facilitate potential targeted follow-up observations of stellar features identified in the survey. Specifically, we anticipate observations to investigate the resolved stellar populations of selected small fields to further explore their origin and structure. We thus require $d < 15$ Mpc (corresponding to distance modulus < 30.9) in order to probe the TRGB of these targeted fields with reasonable integration times using existing instrumentation available on ground-based telescopes and HST.

We impose minimum and maximum angular size constraints to best match our observational mapping strategy to the areal coverage required to trace the extended stellar population ($5 \times R_{25}$, see Section 1.2.2). We exclude small angular extent targets from the sample in order to best match the minimum primary FOV from our mapping strategy ($10' \times 10'$ for an 8×8 grid) with the known optical extent. While this criterion preferentially excludes low mass galaxies from the final sample, our science goals only require a representative sample, with well defined selection criteria, which can then be compared to a sample selected in a similar manner from ΛCDM simulations; thus, a slight over-representation of massive galaxies (relative to the parent sample) is acceptable. The maximum size limit is imposed so that the maximum FOV to be mapped can be accomplished within a single Astronomical Observing Request (AOR). While it is nominally possible to split observations into multiple

AORs to map the large FOVs required for the 7 extremely large nearby galaxies in this survey volume, the potential systematic errors associated with matching sky levels for data taken at different times would pose a significant risk to our science goals. Note that even with these limits, 16 fields require more than 8 hours per AOR.

The above constraints result in a potential sample of 122 galaxies. We examined each field visually to eliminate galaxies that would require masking a significant fraction of the FOV due to either foreground (stars) or background (galaxy clusters) source contamination. We also examined each potential field with SPOT to verify that each target has low infrared sky levels at both 3.6μm and 4.5μm. As expected given the location of these galaxies, the typical expected infrared sky levels for this sample are less than 0.1 MJy sr^{-1} at 3.6μm.

The final target list is a well defined statistically representative sample of normal galaxies within this volume (Figure 4). Our deep observations of a large FOV (at least 5 $\times$ R_{25}) around this representative sample of 92 galaxies will provide an unprecedented view of the faint stellar populations associated with nearby galaxies. **The results of this survey will form the basis for a quantitative statistical analysis comparing observed frequency, distribution, and nature of extended stellar distributions with ΛCDM simulations of galaxy formation.**

1.2.2 Observing Plan

Our observations are designed to map a field of view that corresponds to at least a factor of 5 beyond the bright optical component. The need for wide field mapping observations is driven by the estimated sizes of dark matter halos relative to their bright baryonic components and by the observed extent of the largest gaseous disks currently known. Kinematic tracers indicate that the dark matter halos extend at least a factor of 5 beyond the high surface brightness component for both early- (e.g., Rhode et al. 2007) and late-type galaxies (e.g., Zaritsky et al. 1993; Christlein & Zaritsky 2008). Further, extremely large atomic gas disks (HI-to-optical size ratios of 7-10) have been identified in several low mass dwarf irregular galaxies (e.g, NGC 3741, Begum et al. 2008), indicating that the baryonic component may extend well beyond the high surface brightness regime even in isolated galaxies. Finally, Regan et al. (2006) find smoothly varying stellar surface brightnesses at 3.6μm out to at least $2R_{25}$, the limit of the SINGS data, indicating that deeper observations will reveal a more extended stellar component in most spiral galaxies. Thus, while our proposed observations are exploratory in nature, we expect our observing strategy to sample fully the faint extended stellar distributions for every galaxy.

Astronomical Observing Requests (AORs) are constructed using the successful strategy employed for our Cycle 6 pilot studies. Mosaics are built upon a grid of 100$''$ spacings ($\sim$one-third the IRAC FOV). Two sets of maps will be obtained for each source to enable asteroid removal and to enhance map sensitivity and redundancy. Thus, at any given location within the map cores there will be a total of 18 100s frames resulting in a net integration per sky position of 1800s (along with a 1200s, $\sim$100$''$-wide "inner periphery" and a 600s, $\sim$100$''$-wide "outer periphery"). We will center the mosaics for 3.6μm observations, but even our smallest maps have sufficient sky coverage that the FOV of the corresponding 4.5μm mosaic will include the galaxy as well. We are submitting final AORs for this program. The smallest maps will be 8$\times$8 mosaics, providing 10$'$ map cores at the deepest 1800s effective integration. For highly inclined galaxies, we have modified our mosaic pattern to generate long rectangular strips. To be certain that these rectangular mosaics fully sample the stellar distributions

along the major axis, we apply observing window constraints for 31 rectangular fields (such restrictions are not required for the face-on galaxies as there is no preferred direction for the map); most of these observing constraints are only minor modifications of the source visibility windows and should not substantially effect the flexibility of scheduling the AORs.

As mentioned in Section 1.2.1, we have restricted our sample to include only targets with the lowest possible infrared sky levels (less than 0.1 MJy sr^{-1} at 3.6μm), and thus we expect to achieve a 1σ noise level per pixel of 0.0018 MJy sr^{-1} at 3.6μm for a total integration time of 1800s per pointing (based on both SENS-PET predictions and our Cycle 6 data). Further, the simultaneous images at 4.5μm will have a per pixel surface brightness sensitivity of 0.0027 MJy sr^{-1}; while the 4.5μm mosaic will not be centered on the galaxy, it will both provide an independent observation of the extended stellar distribution and provide the potential to trace the faint stellar population to even larger radii (along the axis of observation).

These deep exposures will allow us to trace the stellar distribution to unprecedented levels of a few $\times$ 0.01 M$_\odot$ pc^{-2} (e.g., Figure 3), at wavelengths that are relatively insensitive to dust and the galaxy's past star formation history. Indeed, the 1800s integration per position on the sky represents a much deeper effort than other surveys of nearby galaxies, e.g., SINGS (240 s), LVL (240 s), S^{4}G (240 s), and the IRAC team GTO project on 100 nearby systems (60 or 150 s; Pahre et al. 2004). These surveys reach a 1σ sensitivity of a few to several kJy sr^{-1}, which is typically at the 5% level with respect to the mid-infrared sky brightness (Regan et al. 2006). With azimuthal averaging, our proposed survey will go down to less than 1 kJy sr^{-1}, a necessity for obtaining high signal-to-noise in the faint outer disks beyond R$_{25}$. For comparison, WISE achieves a 3.4μm sensitivity larger than 1 kJy sr^{-1} over a 5$'$ $\times$ 5$'$ area (Wright et al. 2010).

1.2.3 Data Processing and Analysis

The post-pipeline processing of the data should be straightforward, given our experience with our pilot observations obtained during Cycle 6, as well as our extensive experience with the SINGS and LVL programs. The multi-epoch, multiple-pointing observations for each galaxy will be combined into a single mosaic for each band using the MOPEX mosaicking software. Additional post-BCD processing will include distortion corrections, rotation of the individual frames (for multi-epoch observations), bias structure and bias drift corrections, image offset determinations via pointing refinements from the SSC pipeline, detector artifact removal, constant-level background subtraction, and image resampling to 0.″75 pixels using drizzling techniques. The drizzling slightly improves the final PSF over the native one.

The most significant technical challenge for this project will be the stability of the sky levels within the large FOV and the determination of an accurate sky value for each field. Our pilot projects in Cycle 6 demonstrate that it is possible to obtain high fidelity maps over very large areas during the Warm Mission (we observed sky variations less than 1 kJy sr^{-1} over a 42$'$ $\times$ 39$'$ mosaic in our Cycle 6 observations). Specifically, by mapping the entire field of view during each AOR (two per target), we minimize potential systematic effects from time variability of zodiacal light and thus are able to measure low surface brightness structure on spatial scales larger than the IRAC FOV at the sensitivity levels predicted by SENS-PET (see, e.g., Figures 2 and 3). Furthermore, to minimize sky contamination, we have specifically targeted galaxies with the lowest possible infrared sky brightness as estimated by SPOT. We will measure the sky levels in our post-pipeline processed images by using a curve of growth analysis of azimuthally averaged data prior to measurement of

each galaxy's surface brightness profile. As illustrated in Figures 2 and 3, once the sky level has been determined, azimuthal averages will allow us to probe surface brightness levels well below the single pixel detection limits.

We will examine the derived surface brightness profiles in both 3.6μm and 4.5μm to look for evidence of disk truncation and break radii, as well as to examine the extent of the faint stellar distribution relative to the high surface brightness component. Furthermore, we will create unsharp masked images to identify low mass density stellar streams. Our deep *Spitzer* observations will allow the first quantitative study of the physical properties of such streams (e.g., mass surface density, spatial extent, and total mass associated with each stream) and thus we will be able to explore for the first time fundamental relationships between host galaxy properties and total baryonic mass fraction located in the diffuse stellar distribution. These observations will yield the most extensive and deepest images of the faint stellar populations around nearby galaxies.

In addition to surface brightness profiles, the images will be examined on a point-by-point basis to identify star clusters and background objects. While the images are confusion limited at this depth, we expect the point source catalogs to be dominated by higher redshift galaxies. To discriminate between star clusters and distant galaxies, all bright sources will be compared with data from existing shorter wavelength surveys (such as GALEX, SDSS, and 2MASS). Specifically, moderate depth GALEX FUV and NUV images are available for 49 of the 92 galaxies in this sample (primarily from the NGS and LVL programs, Gil de Paz et al. 2007; Lee et al. 2011) and will provide the basis for initial catalogs of young star cluster candidates. Furthermore, optical images are available for 83 galaxies that lie within the SDSS footprint and for 7 of the 9 southern galaxies (courtesy of LVL; van Zee et al., in prep). These multi-wavelength data sets (from UV to IR) will yield an extensive catalog of star clusters, and will allow us to test the ability of star clusters to remain gravitationally bound at large galactocentric distances.

1.2.4 Enhanced Archival Value

The observations obtained for this project will yield a unique dataset that will lay the foundation for a multitude of studies of the structure and evolution of nearby galaxies. To enhance the archival and legacy value of this project, we will deliver the deep wide-field mosaics produced for our own science applications to the SSC/IRSA for distribution to the astronomical community. The delivery cadence of these high-level science products will be constrained by the observation calendar. Public access to deep wide-field mosaics centered on nearby galaxies will spark a host of new and complementary science applications, beyond those described here.

1.2.5 Management Plan

As PI, van Zee will coordinate the scientific efforts and management of the project. Data processing, including mosaicking and curve of growth analysis, will be led by Dale and Staudaher, who have extensive experience from our pilot observations in Cycle 6 as well as experience from the SINGS and LVL projects. Dale will also serve as technical contact. All team members will participate in data analysis: van Zee and Barnes will lead the analysis of surface photometry of the extended stellar populations, Dalcanton will lead the disk truncations and scale height projects, Calzetti and Dale will lead the disk structure project,

and Chandar will lead the star cluster analysis. Bullock will provide results from N-body simulations and semi-analytic hierarchical galaxy formation models for comparison with observations.

1.3 Figures, Tables & References

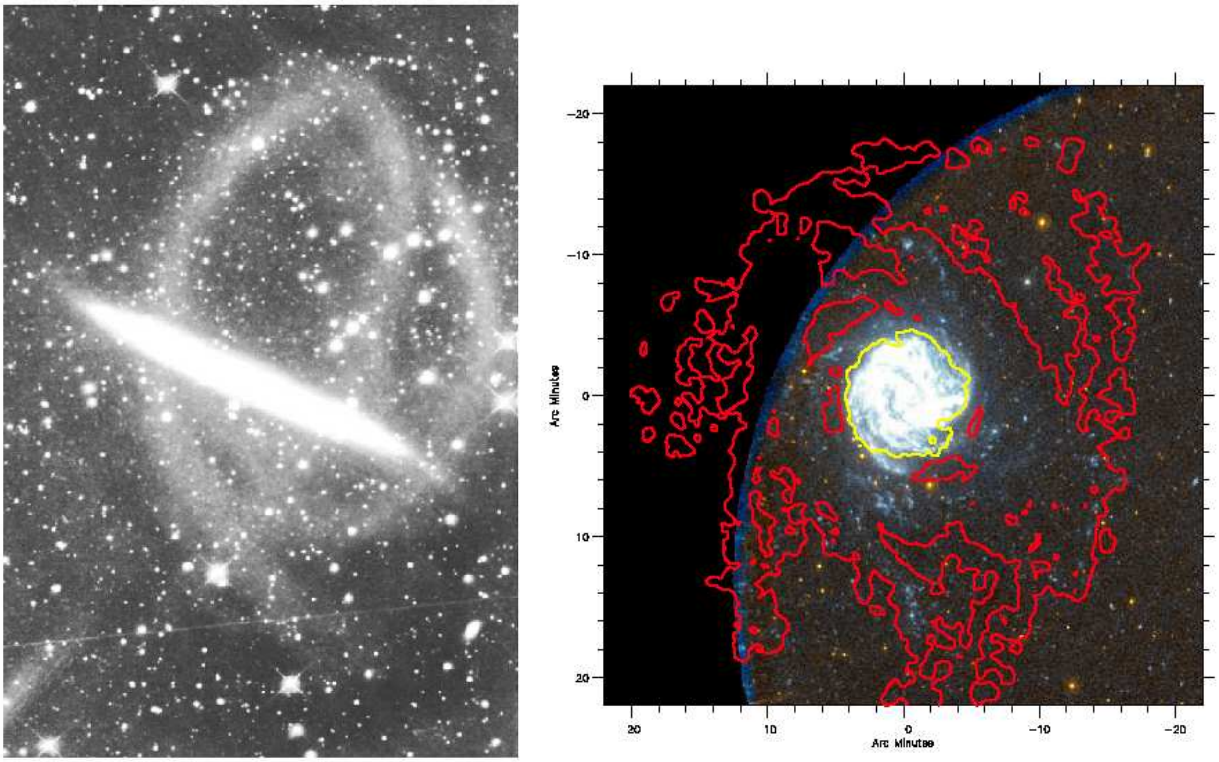

Figure 1: Examples of low surface brightness stellar emission recently identified around spiral galaxies. (*left*) Red low surface brightness stellar emission around NGC5907 was detected with 11.35 hours of integration time on the BBRO 0.5m telescope [Reproduced from Martínez-Delgado et al. 2008]. The diffuse stellar streams around this galaxy can be modelled as the debris created during the accretion of a dwarf satellite. (*right*) The extended UV and HI disk of M83 as seen by GALEX [Reproduced from Thilker et al. 2005]. The extended stellar emission in this galaxy includes a young stellar population and active star formation.

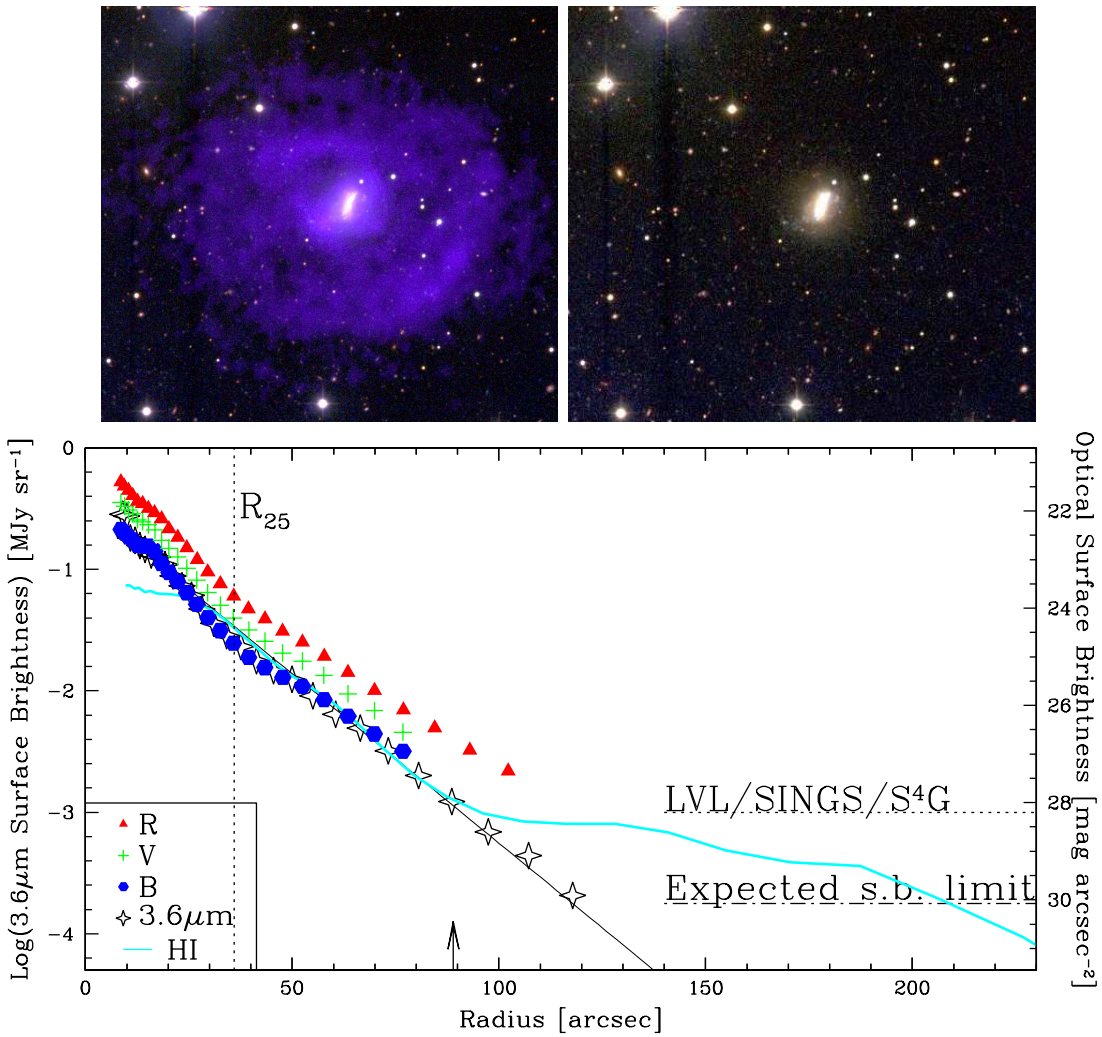

Figure 2: The proposed *Spitzer* observations will probe faint stellar populations to large radii. The power of the proposed IRAC observations is illustrated by a comparison of the surface brightness distribution of UGC 5288, a nearby galaxy with an unusually extended HI disk (top panels), in B (*blue circles*), V (*green plus signs*), R (*red triangles*), 3.6μm (*black stars*), and HI (*cyan solid line*). The optical surface brightness scale (*right side*) has been set so that the B-band and 3.6μm profiles coincide in the outer disk. The optical images were obtained with the KPNO 0.9m (B and V-band) and WIYN 3.5m (R-band); the 3.6μm image is from our Cycle 6 pilot project, which was conducted using the same strategy as proposed here. The theoretical surface brightness limit for these large area (at least 5×R_{25}) deep (1800s) *Spitzer* observations is illustrated. While a 3.3 hour R-band integration on the WIYN 3.5m telescope reaches 27.8 mag arcsec^{-2}, this deep optical image of UGC 5288 is only able to trace the stellar population to a similar radial extent as a short LVL observation (2.5×R_{25}; arrow), and neither are deep enough to probe the stellar mass distribution associated with the break in the HI surface density profile at 90″. Our Cycle 6 IRAC observations reach a full order of magnitude deeper than LVL/SINGS/S^{4}G observations and probe the stellar surface density in the spatial region coinciding with the break in the HI mass surface density profile. Our results indicate that this galaxy has the same exponential stellar mass surface density distribution throughout its entire disk; in other words, the gaseous and stellar surface density profiles diverge at ∼2.5×R_{25} in this system. Deep wide field infrared imaging observations, such as those proposed here, are necessary to trace the faint stellar components of galaxies; thus, our proposed *Spitzer* observations of a statistically representative sample of nearby galaxies will provide unique insight into the formation and growth of galaxy disks.

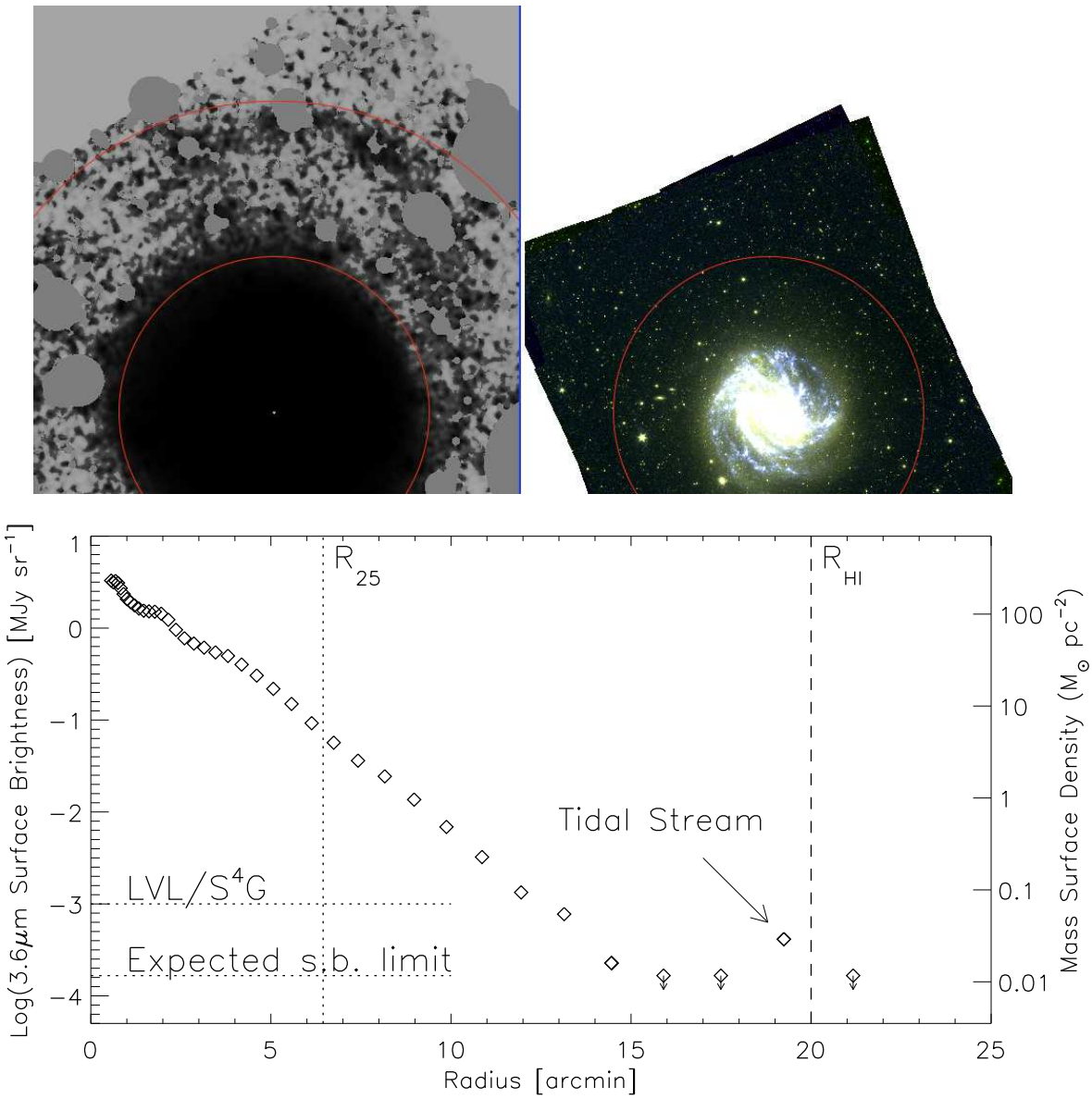

Figure 3: The results of our pilot project to image the extended stellar populations of M83 confirm that our observational strategy yields high fidelity images with the predicted noise characteristics even over large fields of view. The smoothed and masked image in the upper left panel represents a fraction ($31' \times 31'$) of the full ($42' \times 39'$) FOV; the neighboring color image is a composite from previous IRAC observations by the LVL team; red circles of r=$10'$, $20'$ are centered on the galaxy in each image. The observed radial surface brightness profile of M83 traces an extended exponential stellar disk to $15'$ ($\sim$ 20 kpc for a distance of 4.5 Mpc). Furthermore, even the azimuthal average clearly indicates the presence of a stellar stream at $20'$ (first identified by Malin & Hadley 1997); our deep 3.6μm *Spitzer* observations allow us to quantify the stellar surface mass density and total stellar mass associated with this stream for the first time. These observations further indicate that the baryonic component in galaxies can be significantly more extended than an optical image would suggest. With large areal coverage and unprecedented depth, the *Spitzer* observations proposed here will trace faint extended stellar distributions to large radii in a large statistical sample and therefore enable a unique investigation of the statistical properties of the low surface brightness stellar populations associated with nearby galaxies.

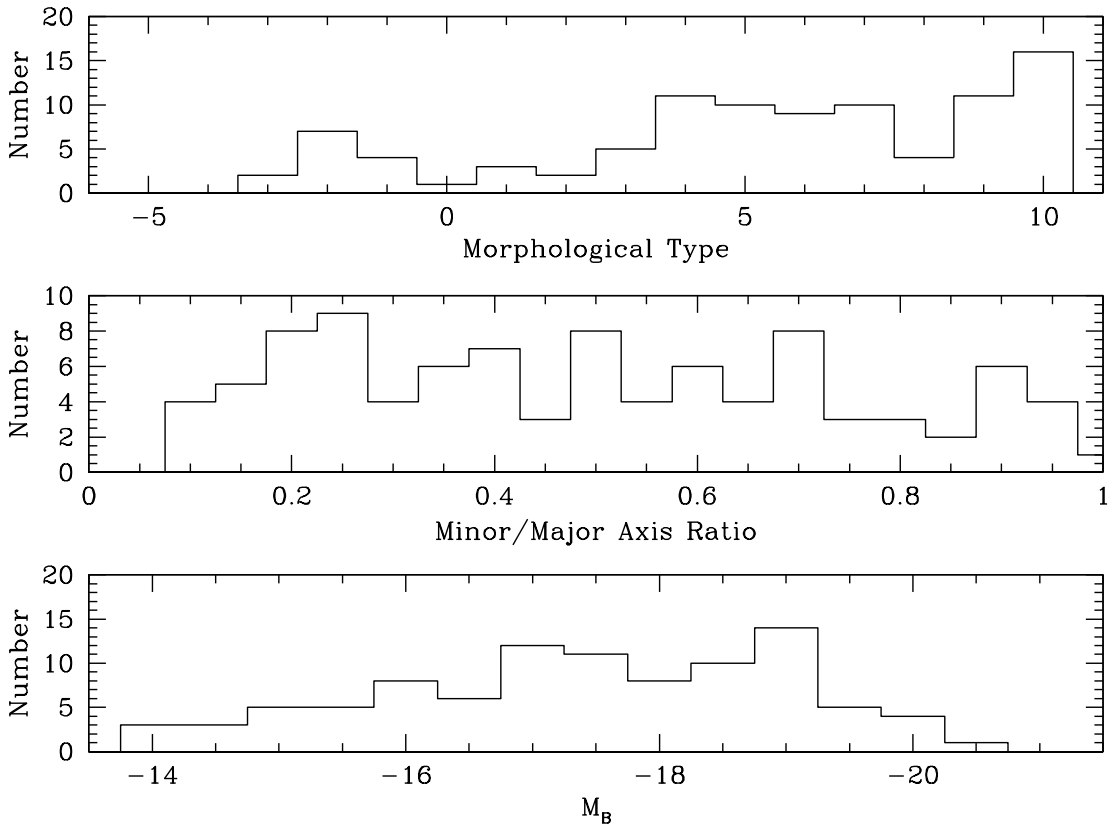

Figure 4: This representative sample of 92 nearby galaxies includes a wide range of morphological types (*top*), axial ratios (*middle*), and optical luminosities (*bottom*). As the proposed observations are exploratory in nature, the sample must include several galaxies of each morphological type and luminosity bin in order to provide a statistically robust result. The volume element of this survey includes a variety of environments from relatively isolated systems to close galaxy pairs and merging systems. Note that the strict galactic latitude constraint $|b| > 60°$ minimizes foreground stellar contamination in the fields, and also results in fields with low infrared sky levels at 3.6μm and 4.5μm, but has no impact on the statistical nature of the sample.

References

Abadi, M. G., Navarro, J. F., & Steinmetz, M. 2006, MNRAS, 365, 747
Alberts, S., et al. 2011, in press
Bakos, J., Trujillo, I., & Pohlen, M. 2008, ApJ, 683, L103
Begum, A., et al. 2008, MNRAS, 383, 809
Bekki, K. 2008, ApJ, 680, L29
Bekki, K., & Chiba, M. 2005, ApJ, 625, L107
Bland-Hawthorn, J., Vlajić, M., Freeman, K. C., & Draine, B. T. 2005, ApJ, 629, 239
Bullock, J. S., & Johnston, K. V. 2005, ApJ, 635, 931
Buta, R., Laurikainen, E., & Salo, H. 2004, AJ, 127, 279
Carignan, C., & Purton, C. 1998, ApJ, 506, 125
Carpenter, J. M. 2000, AJ, 120, 3139
Chandar, R. et al. 2010a, ApJ, 713, 134

Chandar, R. et al. 2010b, ApJ, 719, 966
Christlein, D., & Zaritsky, D. 2008, ApJ, 680, 1053
Dale, D. A. et al. 2009, ApJ, 703, 517
de Jong, R. S. 2008, MNRAS, 388, 1521
de Jong, R. S. et al. 2007, ApJ, 667, L49
Dohm-Palmer, R. C., et al. 1998, AJ, 116, 1227
Dong, H., et al. 2008, AJ, 136, 479
Fall, S. M., Chandar, R., & Whitmore, B. C. 2005, ApJ, 631, L133
Fall, S. M., Chandar, R., & Whitmore, B. C. 2009, ApJ, 704, 453
Ferguson, A. M. N., Wyse, R. F. G., Gallagher, J. S., & Hunter, D. A. 1998, ApJ, 506, L19
Gil de Paz, A. et al. 2007, ApJS, 173, 185
Governato, F. et al. 2007, MNRAS, 374, 1479
Ibata, R., et al. 2007, ApJ, 671, 1591
Ivezić, Z. et al. 2008, ApJ, 684, 287
Johnston, K. V., Sackett, P. D., & Bullock, J. S. 2001, ApJ, 557, 137
Kazantzidis, S., et al. 2008, ApJ, 688, 254
Kennicutt, R. C., et al. 2003, PASP, 115, 928
Kormendy, J., & Kennicutt, R. C. 2004, ARA&A, 42, 603
Kregel, M., & van der Kruit, P. C. 2004, MNRAS, 355, 143
Kregel, M., van der Kruit, P. C., & de Grijs, R. 2002, MNRAS, 334, 646
Kregel, M., van der Kruit, P. C., & Freeman, K. C. 2005, MNRAS, 358, 503
Lada, C. J., & Lada, E. A. 2003, ARA&A, 41, 57
Lee, J. C. et al. 2011, ApJS, 192, 6
Malin, D., & Hadley, B. 1997, PASA, 14, 52
Martínez-Delgado, D., et al. 2008, ApJ, 689, 184
Martínez-Delgado, D., et al. 2010, AJ, 140, 962
Markarian, B. E., Oganesian, E. Ya., & Arakelian, S. N. 1965, Afz., 1, 38
Navarro, J. F., & Steinmetz, M. 2000, ApJ, 538, 477
Pahre, M. A., Ashby, M. L. N., Fazio, G. G., & Willner, S. P. 2004, ApJ, 154, 235
Peñarrubia, J., McConnachie, A., & Babul, A. 2006, ApJ, 650, L33
Pohlen, M., Trujillo, I. 2006, A&A, 454, 759
Regan, M. W., et al. 2006, ApJ, 652, 1112
Rhode, K. L., Zepf, S. E., Kundu, A., & Larner, A. N. 2007, ApJ, 134, 1403
Roškar, R., et al. 2008, ApJ, 675, L65
Sheth, K. et al. 2010, PASP, 122, 1397
Stewart, K. R., et al. 2008, ApJ, 683, 597
Thilker, D. A., et al. 2005, ApJ, 619, L79
Toth, G., & Ostriker, J. P. 1992, ApJ, 389, 5
van den Bosch, F. C. 2001, MNRAS, 327, 1334
van Zee, L., Haynes, M. P., Salzer, J. J., & Broeils, A. H., 1997, AJ, 113, 1618
Wright, E. et al. 2010, AJ, 140, 1882
Yoachim, P., & Dalcanton, J. J. 2006, AJ, 131, 226
Younger, J. D., Cox, T. J., Seth, A. C., & Hernquist, L. 2007, ApJ, 670, 269
Zaritsky, D., & Christlein, D. 2007, AJ, 134, 1053
Zaritsky, D., Smith, R., Frenk, C., & White, S. D. M. 1993, ApJ, 405, 464
Zheng, Z., et al. 1999, AJ, 117, 2757

2 Scheduling Profile of the Proposed Program

We are proposing to observe 92 galaxies in 83 fields located near the Galactic poles. Examining the visibility windows shows that the majority of these fields are optimally viewed between 2011 Jun - Sep, 2011 Dec - 2012 Mar, and 2012 Jun - Sep; approximately 50 to 70 galaxies are visible on any given date within these blocks. Each observation will take between 2 to 20 hours.

3 Brief Team Resume

Liese van Zee (Indiana) is an expert on studies of galaxy formation and evolution with an emphasis on investigating the links between star formation, elemental enrichment, and gas distribution and kinematics in star forming galaxies. She has extensive experience working with multiwavelength data sets (including UV, optical, IR, and radio) and is a co-I on the Local Volume Legacy project (Cycle 4) and PI of our pilot project to examine the faint stellar populations associated with low mass galaxies (Cycle 6).

Danny Dale (Wyoming) is an expert on studies of star formation from low to intermediate redshift and IR properties of galaxies. He has extensive experience with *Spitzer* observations and is a member of both the SINGS and LVL teams.

Kate Barnes (Indiana) is a graduate student at Indiana University. Her PhD dissertation will examine star formation rate indicators in the outer edges of spiral galaxies. She is PI of our pilot project to examine the faint stellar distributions associated with M83.

Shawn Staudaher (Wyoming) is a graduate student at University of Wyoming. He led the IRAC data processing and mosaic construction for the two pilot projects in Cycle 6.

Daniela Calzetti (UMass) is an expert on multiwavelength observations of star formation activity in nearby galaxies. She is a member of both the SINGS and LVL teams.

Julianne Dalcanton (Washington) is an expert on galaxy formation and evolution, including studies of low surface brightness features in nearby galaxies and resolved stellar population studies. She is a member of the LVL team.

James Bullock (Irvine) is an expert on galaxy formation and evolution, including N-body and semi–analytic modelling of hierarchical galaxy formation in a ΛCDM universe.

Rupali Chandar (Toledo) is an expert on multiwavelength studies of star clusters and starburst galaxies.

Selected Related Publications

•*Star Formation in the Outer Disk of Spiral Galaxies: UV and Hα Photometry,* K. Barnes, L. van Zee, and E. Skillman, 2011, ApJ, submitted

•*Spectroscopy of Outlying HII Regions in Spiral Galaxies: Abundances and Radial Gradients,* L. van Zee, et al. 1998, AJ, 116, 2805.

•*Infrared Spectral Energy Distributions of Nearby Galaxies,* D. A. Dale et al. 2005, ApJ, 633, 857.

•*The Spitzer Local Volume Legacy: Survey Description and Infrared Photometry,* D. A. Dale et al. 2009, ApJ, 703, 517.

•*Spitzer Observations of Star Formation in the Extreme Outer Disk of M83 (NGC 5236),* H. Dong, D. Calzetti, et al. 2008, AJ, 136, 479.

4 Summary of Existing Programs

PI L. van Zee is PI of GO-6 program 60094, a 69.7-hour Warm Mission program to probe the older stellar population in the outskirts of galaxies with extended HI disks. The data for this program have been post-pipeline processed and on-going analysis includes developing routines for masking foreground stars and background galaxies, extracting surface brightness profiles, and comparison of stellar and gas surface density distributions.

Co-I K. Barnes is PI of GO-6 program 60116, a 30.2-hour Warm Mission program to probe the extended stellar population in M83. The data for this program have been post-pipeline processed and on-going analysis includes extracting surface brightness profiles and quantifying the physical properties (e.g., mass surface density, spatial extent) of the faint stellar stream and other low surface brightness features.

Co-I D. Dale is Technical contact for the above two programs and is leading the data processing efforts on these two programs.

Co-I Calzetti is PI of 20289 and 30753, Cycle 2 and 3 programs to probe the star formation and dust content in the outer parts of nearby galaxies. Results from the first program are published (Dong et al. 2008) and results from the second project are in press (Alberts et al. 2011).

5 Observation Summary Table

Galaxy Name	Position (J2000)	m_B	$D_{25} \times d_{25}$ (arcmin)	mosaic grid	Hours/ AOR	Observing Constraint
NGC0024	00:09:56.5 −24:57:47	12.38	5.80 × 1.30	18 × 12	6.8	Y
NGC0059	00:15:25.1 −21:26:40	13.12	2.60 × 1.30	9 × 10	2.8	
NGC0625	01:35:04.6 −41:26:10	11.71	5.80 × 1.90	19 × 13	7.7	Y
UGC05829	10:42:41.9 +34:26:56	13.73	4.70 × 4.20	16 × 15	7.5	
NGC3344	10:43:31.2 +24:55:20	10.45	7.10 × 6.50	19 × 22	13.1	
NGC3486	11:00:24.0 +28:58:29	11.05	7.10 × 5.20	22 × 18	12.4	
UGC06112	11:02:35.3 +16:44:05	13.90	2.50 × 0.80	8 × 9	2.2	
NGC3501	11:02:47.3 +17:59:22	13.57	4.76 × 0.54	–	–	
NGC3507	11:03:25.4 +18:08:07	11.73	3.40 × 2.90	14 × 18	7.9	
UGC06161	11:06:49.2 +43:43:24	14.00	2.60 × 1.20	9 × 10	2.8	
UGC06399	11:23:23.2 +50:53:34	14.30	2.48 × 0.61	9 × 10	2.8	
NGC3675	11:26:08.6 +43:35:09	11.00	5.90 × 3.10	11 × 19	6.5	Y
NGC3718	11:32:34.8 +53:04:04	11.59	8.10 × 4.00	20 × 25	15.6	
NGC3729	11:33:49.3 +53:07:32	12.03	2.80 × 1.90	–	–	
NGC3726	11:33:21.2 +47:01:45	10.91	6.20 × 4.30	16 × 20	10.0	Y
NGC3769	11:37:44.1 +47:53:35	12.50	4.10 × 0.82	14 × 12	5.2	
UGC06628	11:40:06.7 +45:56:34	13.18	2.90 × 2.90	11 × 11	3.8	
NGC3893	11:48:38.2 +48:42:39	11.16	4.50 × 2.80	14 × 15	6.6	
UGC06792	11:49:23.3 +39:46:17	14.20	2.80 × 0.40	9 × 10	2.8	
NGC3917	11:50:45.5 +51:49:27	12.51	5.10 × 1.30	16 × 12	6.0	Y
NGC3922	11:51:13.4 +50:09:25	13.40	2.10 × 0.76	8 × 9	2.2	

Galaxy Name	Position (J2000)	m_B	$D_{25} \times d_{25}$ (arcmin)	mosaic grid	Hours/ AOR	Observing Constraint
NGC3938	11:52:49.4 +44:07:15	10.90	5.40 × 4.90	14 × 18	7.9	Y
NGC3941	11:52:55.4 +36:59:11	11.25	3.50 × 2.30	11 × 12	4.1	
NGC3949	11:53:41.4 +47:51:32	11.54	2.90 × 1.70	10 × 11	3.4	
NGC3953	11:53:48.9 +52:19:36	10.84	6.90 × 3.50	11 × 21	7.6	Y
UGC06900	11:55:39.4 +31:31:10	14.80	2.10 × 1.30	8 × 9	2.2	
NGC3972	11:55:45.1 +55:19:15	13.10	3.40 × 0.77	12 × 24	10.4	Y
NGC3998	11:57:56.1 +55:27:13	11.61	2.70 × 2.20	–	–	
UGC06917	11:56:28.8 +50:25:42	13.13	3.50 × 2.00	11 × 12	4.1	
UGC06930	11:57:17.4 +49:16:59	12.65	4.40 × 2.80	14 × 15	6.6	
MESSIER109	11:57:36.0 +53:22:28	10.60	7.60 × 4.70	16 × 24	12.0	Y
UGC06955	11:58:29.8 +38:04:33	13.80	5.00 × 2.60	9 × 17	4.8	Y
NGC4013	11:58:31.4 +43:56:48	12.10	5.20 × 1.00	8 × 17	4.2	Y
IC0749	11:58:34.0 +42:44:02	13.40	2.15 × 1.27	12 × 12	4.5	
IC0750	11:58:52.2 +42:43:21	12.80	2.48 × 0.91	–	–	
NGC4010	11:58:37.9 +47:15:41	13.20	3.17 × 0.73	9 × 11	3.1	
UGC06983	11:59:09.3 +52:42:27	13.12	3.50 × 2.40	11 × 12	4.1	
NGC4026	11:59:25.2 +50:57:42	11.67	5.20 × 1.30	8 × 17	4.2	Y
NGC4051	12:03:09.6 +44:31:53	10.83	5.20 × 3.90	17 × 14	7.4	Y
NGC4068	12:04:00.8 +52:35:18	13.00	3.30 × 1.70	10 × 12	3.8	
NGC4085	12:05:22.7 +50:21:10	12.95	2.80 × 0.80	–	–	
NGC4088	12:05:34.2 +50:32:20	11.15	5.80 × 2.20	14 × 22	9.6	
UGC07089	12:05:58.1 +43:08:43	14.00	2.75 × 0.67	19 × 20	11.9	
NGC4111	12:07:03.1 +43:03:55	11.63	4.60 × 1.00	–	–	
NGC4096	12:06:01.1 +47:28:42	12.30	4.39 × 1.04	8 × 15	3.8	Y
NGC4100	12:06:08.1 +49:34:59	11.89	5.40 × 1.80	8 × 18	4.5	Y
NGC4102	12:06:23.1 +52:42:39	11.99	2.70 × 1.00	9 × 10	2.8	
UGC07125	12:08:42.3 +36:48:10	14.10	3.11 × 0.62	10 × 11	3.4	
NGC4138	12:09:29.8 +43:41:07	12.16	2.60 × 1.70	9 × 10	2.8	
NGC4143	12:09:36.1 +42:32:03	11.65	2.30 × 1.40	8 × 9	2.2	
NGC4144	12:09:58.6 +46:27:26	12.05	6.00 × 1.30	19 × 12	7.1	Y
NGC4151	12:10:32.6 +39:24:21	11.50	6.30 × 4.50	18 × 20	11.2	
NGC4183	12:13:16.9 +43:41:55	12.90	6.39 × 0.69	20 × 12	7.5	Y
NGC4203	12:15:05.0 +33:11:50	11.80	3.40 × 3.20	12 × 12	4.5	
NGC4214	12:15:39.2 +36:19:37	10.24	8.50 × 6.60	23 × 26	18.7	
NGC4220	12:16:11.7 +47:53:00	12.20	3.84 × 0.92	12 × 13	4.9	
UGC07301	12:16:42.1 +46:04:44	15.30	2.19 × 0.33	8 × 9	2.2	
NGC4242	12:17:30.2 +45:37:10	11.37	5.00 × 3.80	14 × 17	7.4	Y
UGC07408	12:21:15.0 +45:48:41	13.35	2.60 × 1.20	9 × 10	2.8	
NGC4369	12:24:36.2 +39:22:59	12.33	2.10 × 2.00	8 × 9	2.2	
NGC4389	12:25:35.1 +45:41:05	12.60	2.14 × 1.36	8 × 9	2.2	
UGC07577	12:27:40.9 +43:29:44	12.84	4.30 × 2.40	24 × 16	12.0	Y
UGC07608	12:28:44.2 +43:13:27	13.67	3.40 × 3.30	–	–	

Galaxy Name	Position (J2000)	m_B	$D_{25} \times d_{25}$ (arcmin)	mosaic grid	Hours/ AOR	Observing Constraint
NGC4460	12:28:45.6 +44:51:51	12.26	4.00 × 1.20	12 × 14	5.2	
UGC07639	12:29:53.4 +47:31:52	14.30	2.30 × 1.60	8 × 9	2.2	
NGC4485	12:30:31.1 +41:42:04	12.32	2.30 × 1.60	–	–	
NGC4490	12:30:36.4 +41:38:37	10.22	6.30 × 3.10	20 × 13	8.1	Y
UGC07699	12:32:48.0 +37:37:18	13.30	2.84 × 0.78	10 × 11	3.4	
UGC07774	12:36:22.7 +40:00:19	14.50	2.83 × 0.43	9 × 10	2.8	
NGC4618	12:41:32.8 +41:09:03	11.22	4.20 × 3.40	13 × 14	5.7	
IC3687	12:42:15.1 +38:30:12	13.71	3.40 × 3.00	11 × 12	4.1	
NGC4707	12:48:22.9 +51:09:53	13.40	2.20 × 2.10	9 × 9	2.5	
NGC4861	12:59:02.3 +34:51:34	12.90	4.00 × 1.50	10 × 14	4.4	Y
IC4182	13:05:49.5 +37:36:18	13.00	6.00 × 5.50	19 × 20	11.9	
NGC5005	13:10:56.2 +37:03:33	10.61	5.80 × 2.80	10 × 19	5.9	Y
IC4213	13:12:11.2 +35:40:11	14.01	2.50 × 0.50	9 × 10	2.8	
NGC5023	13:12:12.6 +44:02:28	12.85	7.28 × 0.78	8 × 23	5.8	Y
NGC5033	13:13:27.5 +36:35:38	10.75	10.70 × 5.00	16 × 28	14.0	Y
UGC08303	13:13:17.6 +36:13:03	13.48	2.20 × 1.90	–	–	
UGC08320	13:14:28.0 +45:55:09	12.70	3.60 × 1.40	11 × 13	4.5	
MESSIER063	13:15:49.3 +42:01:45	9.31	12.60 × 7.20	29 × 22	20.0	Y
NGC5229	13:34:02.8 +47:54:56	14.30	3.58 × 0.45	8 × 12	3.0	Y
NGC5273	13:42:08.3 +35:39:15	12.44	2.80 × 2.50	10 × 11	3.4	
UGC08839	13:55:24.9 +17:47:43	13.60	4.00 × 2.70	14 × 12	5.2	
NGC5523	14:14:52.3 +25:19:03	12.75	4.60 × 1.30	15 × 10	4.7	Y
NGC5608	14:23:17.9 +41:46:33	13.90	2.60 × 1.30	9 × 10	2.8	
ESO290-G028	22:57:09.0 −42:48:16	14.50	5.11 × 0.50	17 × 8	4.2	Y
NGC7713	23:36:15.0 −37:56:17	11.50	4.50 × 1.80	8 × 15	3.8	Y
UGCA442	23:43:45.6 −31:57:24	13.60	6.38 × 0.90	20 × 10	6.2	Y
ESO348-G009	23:49:23.5 −37:46:19	13.60	2.40 × 1.00	8 × 9	2.2	
ESO149-G003	23:52:02.8 −52:34:40	15.00	2.20 × 0.40	8 × 9	2.2	
NGC7793	23:57:49.8 −32:35:28	9.98	9.30 × 6.30	28 × 20	18.0	Y

The above sample includes nine galaxy pairs/groups for which it is more efficient and scientifically relevant to make a single map that includes all target galaxies: (1) NGC3507/01 will be centered between the galaxies; (2) NGC3718/29 will be centered on NGC3718; (3) NGC3972/90/98 will be centered between the galaxies; (4) IC0749/50 will be centered between the galaxies; (5) NGC4085/88 will be centered between the galaxies; (6) UGC07089/UGC07084/NGC4111/NGC4117 will be slightly offset from UGC07089; (7) UGC07557/7608 will be centered between the galaxies; (8) NGC4485/90 will be centered on NGC4490; (9) NGC5033/UGC08308 will be centered between the galaxies.

There are 1005.3 hrs total requested for this observing program.

6 Modification of the Proprietary Period

No proprietary period is requested.

7 Summary of Duplicate Observations

There are no duplicate observations. While almost all of the galaxies in this sample have been observed at 3.6μm and 4.5μm previously with *Spitzer*, all previous IRAC observations have significantly shorter integration times and include a smaller field of view than proposed here. Specifically, previous observations by the SINGS (P00159), LVL (P40204), and S^{4}G (P61060-8) programs have neither the depth (2×4×30 s/pix = 240 s/pix) nor field–of–view (only 1.5-2.5 × R_{25}) to be considered as duplications.

8 Summary of Scheduling Constraints/ToOs

We are constraining the timing window for 31 fields for which we desire the rectangular mosaics to be aligned within 15 degrees of the galaxy's major axis. All windows are at least two weeks long and the majority of these timing windows are three to four weeks long (i.e., at least half of the original visibility window). Sixteen fields (32 AORs) are in excess of 8 hours.